ELSEVIER

Thermochimica Acta 324 (1998) 109–121

thermochimica acta

Modulated differential scanning calorimetry: 13. Analysis of morphology of poly(ethyl methacrylate)/polyurethane interpenetrating polymer networks

D.J. Hourston[a,*], M. Song[a], F.-U. Schafer[a], H.M. Pollock[b], A. Hammiche[b]

[a] *IPTME, Loughborough University, Loughborough LE11 3TU, UK*
[b] *School of Physics and Chemistry, Lancaster University, Lancaster LA1 4YB, UK*

Abstract

The phase structure of poly(ethyl methacrylate)–polyurethane (PEMA/PUR) interpenetrating polymer networks (IPNs) has been investigated by means of modulated-temperature differential scanning calorimetry (M-TDSC), dynamic mechanical thermal analysis (DMTA) and small-angle X-ray scattering (SAXS). Experimental data from both M-TDSC and SAXS indicate that the morphologies of all the PEMA/PUR IPN samples (90 : 10 to 10 : 90 PUR/PEMA) are multi-phase structures. The scattering peaks from SAXS are quite broad, thereby indicating a distribution of microdomain sizes from 5 to 12 nm. This structure formation in IPNs is a competitive process between phase separation and the formation of cross-links which restricts segmental diffusion. An M-TDSC-based characterization method for IPNs has been developed using the differential of heat capacity signal, dC_p/dT, to analyze phase structure and calculate the weight fraction of each component.

Keywords: Glass transition; Interpenetrating polymer networks; Modulated-temperature DSC; Small-angle X-ray scattering

1. Introduction

An interpenetrating polymer network (IPN) is defined as a combination of two cross-linked polymers, at least one of which has been synthesised and or cross-linked in the immediate presence of the other. From the topological point of view, IPNs are closely related to polymer blends, block, graft and cross-linked copolymers. An IPN can be distinguished from other multi-phase polymer systems in three ways:

1. in the presence of solvents an IPN swells, but does not dissolve;
2. creep and flow are suppressed; and
3. as a result of mutual incompatibility, IPNs exhibit characteristic morphologies.

From the synthesis point of view, IPNs are of two types.

(a) Polymer network 1 is swollen with the monomers and cross-linker of the second polymer which is then polymerized in situ – such a material is called a sequential IPN.
(b) Both the networks are synthesized simultaneously by independent, non-interfering routes – the product is called a simultaneous interpenetrating network.

If one of the two polymers is linear (uncross-linked), a semi-IPN results. A homo-IPN results if both the network polymers are the same [1].

Since the second polymer is still in monomeric form when it is mixed with the first polymer in a sequential IPN synthesis, there is still a considerable entropy of mixing. Upon polymerization, the entropy of mixing

*Corresponding author.

0040-6031/98/$ – see front matter
PII: S0040-6031(98)00528-0

is greatly decreased and phase separation [1] usually occurs. The vast majority of IPNs are phase separated, multi-phase materials. Intuitively, the networks formed in the first and/or second polymerization should limit the extent of phase separation and give control of domain size and the extent of mixing of the two components. It is important to know the morphology of IPNs and the factors influencing it, since domain size and shape of the phase, interface bonding and phase connectivity determine the physical and mechanical properties of such materials. The size, shape, connectivity and interfacial characteristics of the phase-separated zones vary according to the particular system and its mode of synthesis. Together, these parameters combine to describe the morphology of the IPNs, which is, generally, rather complicated and has been the subject of many studies [2,3]. Most research results show that during polymerisation, two competing processes take place simultaneously. Phase separation of the forming polymer chains proceeds by diffusion through an increasingly viscous media to form phase domains. The formation of cross-links restricts this diffusion and, at gelation, the then present situation is substantially frozen in. Consequently, phase separation in IPNs depends primarily on

(i) the miscibility of the constituent polymers;
(ii) the cross-link density in both polymer networks and any inter-network grafting;
(iii) the reaction conditions (temperature, pressure); and
(iv) the relative reaction rates of network formation.

With highly incompatible polymers, the thermodynamic driving force for phase separation is so powerful that gross phase separation occurs before gelation [1]

Frisch et al. [4] were the first to synthesize IPNs from polymers that form compatible blends. They were based on polystyrene and polyphenylene oxide. Evidence for miscibility was based on differential scanning calorimetry, DSC, and dynamic mechanical thermal analysis, DMTA, measurements, which showed a single glass-transition temperature, and electron microscopy which showed no evidence of phase separation. The influences of hydrogen bonding [5] and cross-linking [6,7] on morphology have also been discussed in the literature.

Among the techniques that are widely used to investigate the IPN morphology are DSC [4], transmission electron microscopy, TEM [1], scanning electron microscopy [8] and DMTA [1]. To a lesser extent, small-angle neutron scattering [9], small-angle X-ray scattering, SAXS [10], and dielectric measurements [11] are also used.

In this paper, modulated-temperature differential scanning calorimetry, M-TDSC, and SAXS techniques are used to study the morphology of poly(ethylmethacrylate)–polyurethane (PEMA/PUR) IPNs.

2. Experimental

2.1. Materials

Polyoxypropylene glycol of a molar mass 1025 (PPG1025) was used as the polyurethane (PUR) soft segment. The hard segment was formed from 1,1,3,3-tetramethylxylene diissocyanate (TMXDI) and the cross-linker was trimethylol propane (TMP). Stannous octoate (SnOC) was used as the PUR catalyst. Polyethyl methacrylate (PEMA) was formed by cross-linking ethyl methacrylate monomer (EMA) with tetraethyleneglycol dimethacrylate(TEGDM). Azoisobutyronitile (AIBN) was used as the initiator.

The TMP was dissolved in the PPG1025 at 60°C. At room temperature, the EMA, TEGDM and the dissolved AIBN were added. Upon addition of the SnOC and the TMXDI, the components were stirred under a nitrogen blanket for 5 min. After degassing for 1 min at high vacuum, the mixture was moulded in an O-ring mould. Curing was conducted in three cycles of 24 h at 60°, 80° and 90°C. The sample codes used for the PUR/PEMA IPN series are shown in Table 1.

2.2. M-TDSC theory

A TA Instruments M-TDSC was used. An oscillation amplitude of 1.0°C and an oscillation of 60 s period were used at a heating rate of 3°C/min. The calorimeter was calibrated with indium and sapphire standards.

The theoretical background to M-TDSC analysis in the glass-transition region in now briefly described. A differential equation to describe the kinetics of enthalpy (H) relaxation for conventional differential

Table 1
Sample codes for the PUR/PEMA IPN series

System	PUR (wt.%)	PEMA
PEMA100	0	100
PEMA90	10	90
PEMA80	20	80
PEMA70	30	70
PEMA60	40	60
PEMA50	50	50
PEMA60	60	40
PEMA30	70	30
PEMA20	80	20
PEMA10	90	10
PUR100	100	0

scanning calorimetry (DSC) has been proposed by Kovacs and Hutchinson [12].

$$d\delta/dt = \Delta C_p q - \delta/\tau(T,\delta) \quad (1)$$

In this equation, $\delta(=H-H_\infty)$ is the excess enthalpy relative to the equilibrium value (H_∞), ΔC_p the difference between the liquid ($C_{p,l}$) and glass state ($C_{p,g}$) specific heat capacities, q the heating rate and t the time.

The single relaxation time τ depends [12] on both, T and δ according to Eq. (2).

$$\tau = \tau_g \exp[-\theta(T-T_g)]\exp[-(1-x)\theta\delta/\Delta C_p] \quad (2)$$

where τ_g is the equilibrium relaxation time at the glass-transition temperature T_g, x the non-linearity parameter ($0 \le x \le 1$), and θ a constant defining the temperature dependence of τ which is given by the following approximation

$$\theta = \Delta h^*/(RT_g^2) \quad (3)$$

Here, Δh^* is an apparent activation energy. Eqs. (1) and (2) define the response of the glass to any prescribed thermal history. For simplicity, the following approximate equation will be used in this paper for the relaxation time τ

$$\tau = \tau_g \exp[-\theta(T-T_g)] \quad (4)$$

In M-TDSC, the basic idea is to superimpose upon the conventional DSC heating rate a periodically varying temperature modulation. This modulation is sinusoidal, giving a time-dependent temperature [13].

$$T = T_0 + qt + A_T \sin(\omega t) \quad (5)$$

where T_0 is the initial temperature of the DSC scan, A_T the amplitude of temperature modulation, and ω the frequency of modulation.

Using the variable $\eta = \delta + T\Delta C_p$, Lacey et al. [14] made approximations to Eq. (1), which leads to the following equations:

$$\begin{aligned} d\eta/dt &= \exp[\Delta h^*/(RT_g^2)(T-T_g)] \\ &\quad \times (T\Delta C_p - \eta)/\tau_g \\ &= [\Delta C_p qt + A_T \Delta C_p \sin(\omega t) - \eta] \\ &\quad \times \exp[Kqt + KA_T \sin(\omega t)]/\tau_0 \end{aligned} \quad (6)$$

$$\tau_0 = \exp(\Delta h^*/RT_g)\tau_g \quad (7)$$

For M-TDSC, Lacey et al. [14] proposed that $\eta = \langle\eta\rangle + A_T \mathrm{Re}\{\phi \exp(i\omega t)\}$. $\langle\eta\rangle$ is the underlying (principal) part of η.

$$d\langle\eta\rangle/dt = [\Delta C_p qt - \langle\eta\rangle]\exp(Kqt)/\tau_0 \quad (8)$$

where ϕ is the 'complex amplitude' [14].

$$\begin{aligned} i\omega\phi\exp(i\omega t) &= \exp(i\omega t)[K\Delta C_p qt - \langle\eta\rangle) \\ &\quad + \Delta C_p]\exp(Kqt)/\tau_0 \\ &\quad - \exp(Kqt)/\tau_0 \phi \exp(i\omega t) \end{aligned} \quad (9)$$

Then,

$$\begin{aligned} \langle\eta\rangle &= A\exp[-e^{Kqt}/(Kq\tau_0)] + qt\Delta C_p - q\Delta C_p \\ &\quad \times \exp[-e^{Kqt}/(Kq\tau_0)] \int_0^t \exp[e^{Kqt}/(Kqt_0)]dt' \end{aligned} \quad (10)$$

and

$$\begin{aligned} \phi = i\{&K(\langle\eta\rangle - qt\Delta C_p) - \Delta C_p]/ \\ &[1 + i\omega\tau_0 \exp(-Kqt)] \end{aligned} \quad (11)$$

For M-TDSC [15],

$$\begin{aligned} dQ/dt &= C_{pt} dT/dt + f(t,T) \\ &= qC_{pt} + \langle f(t,T)\rangle \\ &\quad + \omega A_T C_p t\cos(\omega t) + C\sin(\omega t) \end{aligned} \quad (12)$$

dQ/dt is the heat flow into the sample, C_{pt} the reversing heat capacity of the sample due to its molecular motions at the heating rate q, $f(t,T)$ is the heat flow arising as a consequence of a kinetically retarded

event, $\langle f(t,T)\rangle$ the average of $f(t,T)$ over the interval of at least one modulation and C the amplitude of the kinetically retarded response to the temperature modulation.

Consider the complex heat capacity, C_p^*

$$C_p^* = A_{HF}/A_q \tag{13}$$

A_{HF} and A_q are the amplitudes of heat flow and heating rate, respectively.

The complex heat capacity is out of phase with the heating rate, and a real part, C_p', and an imaginary part, C_p'' may be assigned as follows:

$$C_p' = C_p^*\cos\alpha \text{ and } C_p'' = C_p^*\sin\alpha \tag{14}$$

$$C_p^* = C_p' - iC_p'' \tag{15}$$

Here, α is the phase angle between heat flow and heating rate.

Also, the following equations may be written [13]:

$$dQ/dt \equiv C_{pt}dT/dt + f(t,T) = qC_{pt} + \langle f(t,T)\rangle + \omega A_T C_{p\omega}\cos(\omega t) + C\sin(wt) \tag{16}$$

$C_{p\omega}$ is the reversing heat capacity at the frequency ω.

Since $dQ/dt = C_{pg}dT/dt + d\eta/dt$, we have [14]

$$qC_{pt} + \langle f(t,T)\rangle = qC_{pg} + d\langle\eta\rangle/dt \tag{17}$$

and

$$\omega A_T C_{p\omega}\cos(\omega t) + C\sin(\omega t) = [(C_{pg} - \mathrm{Im}\{\phi\}\cos(\omega t) - \mathrm{Re}\{\phi\}\sin(\omega t)] \tag{18}$$

Assuming $C_p' = A + BT + F(T)$ during the glass transition, according to Lacey et al. [14], C_p' and C_p'' can be obtained as follows:

$$C_p' = A + BT + \Delta C_p(1 - \exp(-\Delta h^* T/(RT_g^2))/(1 + \omega^2\tau_g^2\exp(-2\Delta h^*/(RT_g^2)(T - T_g))) \tag{19}$$

$$C_p'' = \Delta C_{p\omega}\tau_g\exp(-\Delta h^*/(RT_g^2)(T - T_g))(1 - \exp(-\Delta h^* T/RT_g^2))/(1 + \omega^2\tau_g^2\exp(-2\Delta h^*/(RT_g^2)(T - T_g))) \tag{20}$$

Figs. 1 and 2 show C_p', C_p'' and $\tan\delta$ vs. temperature for polystyrene. For this theoretical analysis, the following parameters were used:

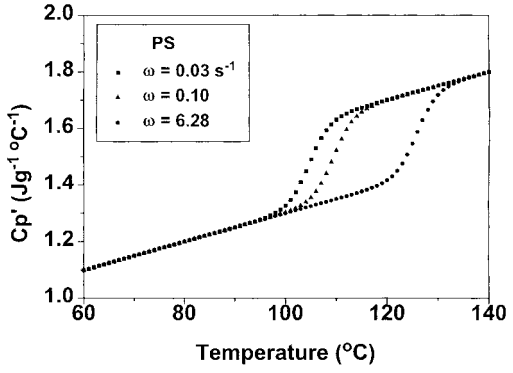

Fig. 1. Theoretical C_p' vs. temperatures curves for polystyrene at different frequencies.

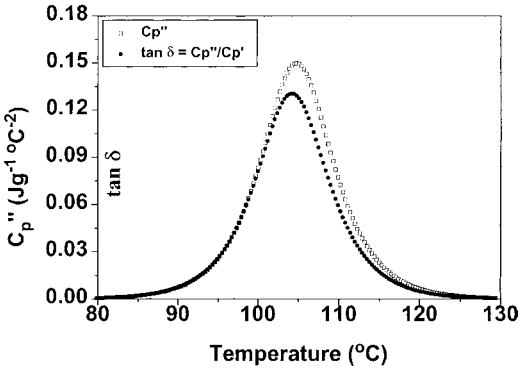

Fig. 2. Theoretical C_p'' and $\tan\delta$ vs. temperature curves in the glass-transition region for polystyrene.

$\Delta C_p = 0.3\,\mathrm{Jg^{-1}\,°C^{-1}}$	(Ref. [12])
$\Delta h^* = 300\,\mathrm{kJ/mol}$	(assumed value)
$A = 0.8\,\mathrm{Jg^{-1}}$	(assumed value)
$B = 0.002\,\mathrm{Jg^{-1}\,°C^{-1}}$	(assumed value)
$\tau_g = 100\,\mathrm{s}$	(Ref. [12])

Figs. 3 and 4 are a comparison of dC_p'/dT vs. temperature data for experimental, theoretical and a Gaussian function for polystyrene and a 50/50 weight blend of poly(methyl methacrylate) and poly(styrene-co-acrylonitrile) [16]. Obviously, the experimental data at the glass transition can be described by the theory, and also well remain, by a Gaussian function. For simplicity, in this paper, we use a Gaussian function to describe the change of dC_p'/dT vs. temperature at the glass transition.

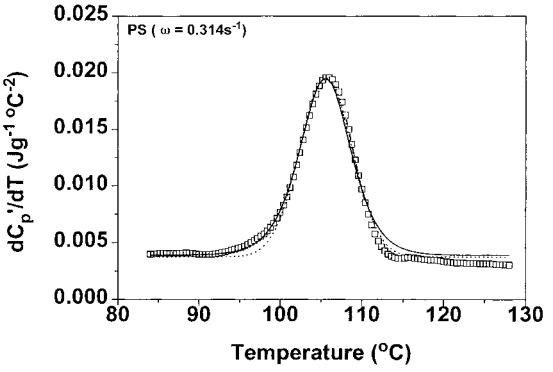

Fig. 3. dC_p'/dT vs. temperature data for polystyrene. Experimental data (squares), theoretical plot (solid line) and a Guassian function (dotted line).

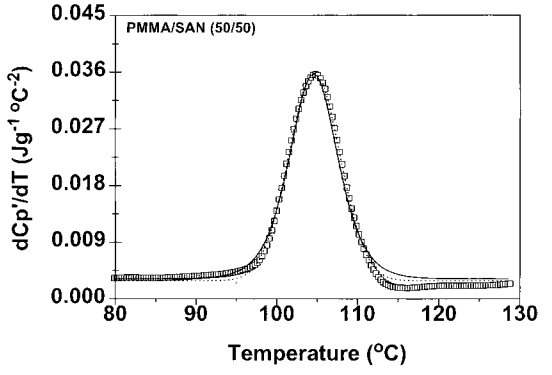

Fig. 4. dC_p'/dT vs. temperature data for a miscible blend of poly(methyl methacrylate) and poly(styrene-co-acrylonitrile) (50/50 by weight). Experimental data (squares), theoretical plot (solid line) and a Gaussian function (dotted line).

2.3. SAXS measurements

The SAXS measurements were performed with a Kratky Compact camera (Paar KG) equipped with a one-dimensional position-sensitive detector (Braun). Ni-filtered CuK_a radiation (λ=0.154 nm) was used. The sample was kept in the camera under vacuum to minimise air scattering. All data were taken at room temperature. They were corrected for absorption, background scattering, slit length smearing and thermal fluctuation. Primary beam intensities were determined in absolute units [e.u^2/nm^3] by using a moving slit method.

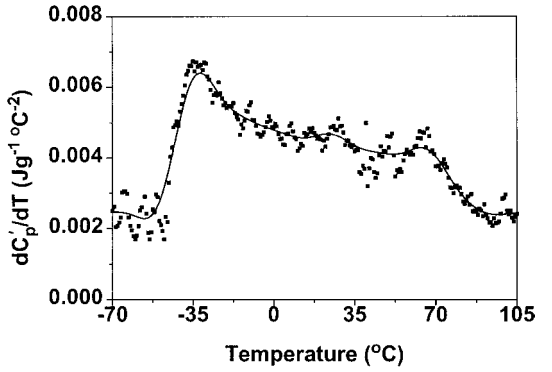

Fig. 5. Raw (squares) and smoothed (solid line) dC_p/dT vs. temperature data for the PEMA60 IPN.

2.4. Dynamic mechanical thermal analysis (DMTA)

The testing mode chosen for this study was the single cantilever bending configuration. Samples in the form of a bar with typical dimensions of $30\times10\times3$ mm^3 were used. The samples were analysed in the temperature range between -60° and 200°C at a heating rate of 3°C/min. The frequency chosen was 10 Hz. A Polymer Laboratories instrument was used.

2.5. Curve synthesis and analysis of overlapping spectral features

A new signal, the differential of heat capacity, dC_p'/dT, was developed in this work. Fig. 5 gives an example for the change of dC_p'/dT with temperature for the PEMA60 IPN. Obviously, the signal in glass transition region is quite complex. Analysing the signal needs curve synthesis and multi-peak resolution techniques.

Nearly all data systems provide a smoothing facility. Such an operation must be carried out with care and this section is concerned with the effect that smoothing has upon data and suggests how smoothing might be carried out in the most effective and least distorting way. In general, it is always much better to use unsmoothed data, since any smoothing procedure is bound to introduce some sort of distortion to the curve. However, when the dC_p'/dT signal is used, there is significant noise. There are many cases where some smoothing is required. Smoothing is a process that

attempts to increase the correlation between points while suppressing uncorrelated noise. Smoothing is achieved by convolution of data with a suitable smoothing function. The least-squares central-point smoothing techniques proposed by Savisky and Golay [17] were used in this work. Fig. 5 (solid line) shows how the method can be successfully applied to typical dC'_p/dT data for a multi-component polymer system. Compared with the raw data, the smoothed spectrum contains no new information. The smoothed curve makes some curve features more evident, and is thus more useful than the unsmoothed spectrum.

3. Results and discussion

3.1. Glass transition behaviour of the IPNs

It has been found [18] that with pairs of semi-compatible polymers, IPNs with very fine micro-heterogeneous morphologies and phase domains in the order of 5–30 nm, can be obtained. In this paper, the morphologies of the PUR/PEMA IPNs of varying composition were investigated. Both the polymers contain groups which are polar and their solubility parameters, determined by equilibrium swelling [19], are 20.3 $(J/m^3)^{1/2}$ for the PUR and 18.0 $(J/m^3)^{1/2}$ for the PEMA. The dC'_p/dT signal and DMTA data are interpreted in terms of morphology and miscibility of the component networks.

In tan δ vs. temperature plots of polymer blends, one narrow loss peak indicates a high degree of miscibility, whereas two clearly separated tan δ transitions with low inter-transition tan δ values are indicative of gross phase separation. The tan δ vs. temperature data for both homo-networks and selected IPN compositions are shown in Fig. 6(a and b). A single-transition peak was obtained for the 90 : 10, 80 : 20, 30 : 70, 20 : 80 and 10 : 90 IPN compositions. The intermediate compositions between 70 : 30 and 40 : 60 revealed phase separation to some extent and exhibited a shoulder at the second transition. The 50 : 50 composition showed three transitions, one main peak at 88°C with two shoulders at 27°C and −10°C, respectively. A similar phenomenon has been previously reported [20,21] for polyurethane/poly-(methyl methacrylate) IPNs and was explained by the presence of a substantial interphase region.

Detailed information about the morphology of the PUR/PEMA IPNs can be obtained from the dC'_p/dT vs. temperature signals. The dC'_p/dT vs. temperature data for both homo-networks and selected IPN compositions are shown in Fig. 7(1–8). From these M-TDSC results, it can be concluded that the morphologies of the 80 : 20, 70 : 30, 60 : 40, 50 : 50, 40 : 60 (see Fig. 5), 30 : 70 and 20 : 80 PUR/PEMA IPNs are multiphase structures. Comparing the dC'_p/dT signals of the PUR 100 and the PUR90, it was found that a shoulder exists on the PUR90 transition. For the PEMA90 system, between −30 and 20°C, there exists a weak, broad transition. Hence, this multi-phase behaviour over the entire composition range in the PUR/PEMA IPNs seems to be confirmed by the M-TDSC measurements.

Transmission electron (TEM) micrographs of the different compositions corroborated the findings from the DMTA and M-TDSC measurements. For all compositions, no gross phase separation was observed [22]. The phase domains were not well defined, but appeared to show gradual change in composition. The 90 : 10 and 80 : 20 PUR/PEMA IPNs were difficult to ultramicrotome, because of their softness at room temperature. The micrographs showed a very fine morphology with PEMA domains in the order of 5–40 nm in the OsO_4-stained PUR matrix. For the 20 : 80 PUR/PEMA IPN composition, the PUR domains were only just resolvable by TEM [22]. The PUR domains were in the order of 1–10 nm [22]. TEM micrographs confirmed the M-TDSC results. During IPN formation, phase separation of constituent networks takes place due to increasing thermodynamic incompatibility during the course of curing.

The T_g, obtained from M-TDSC, vs. composition plots for the PUR-rich and PEMA-rich phases are shown in Fig. 8. It can be seen that the T_g values of the PUR networks remain essentially constant at the 40 : 60, 50 : 50, 60 : 40, 70 : 30, 80 : 20 and 90 : 10 compositions. The T_g values of PUR networks in the IPNs are similar to that of the pure PUR network. However, the T_g values of the PEMA networks are lower by at least 15°C than that (76°C) of the pure PEMA network. For uncross-linked PEMA, the T_g value was ca. 68°C. Obviously, the decrease in the T_g values did not result only from a decrease of cross-link densities in the IPNs compared to the homo-networks.

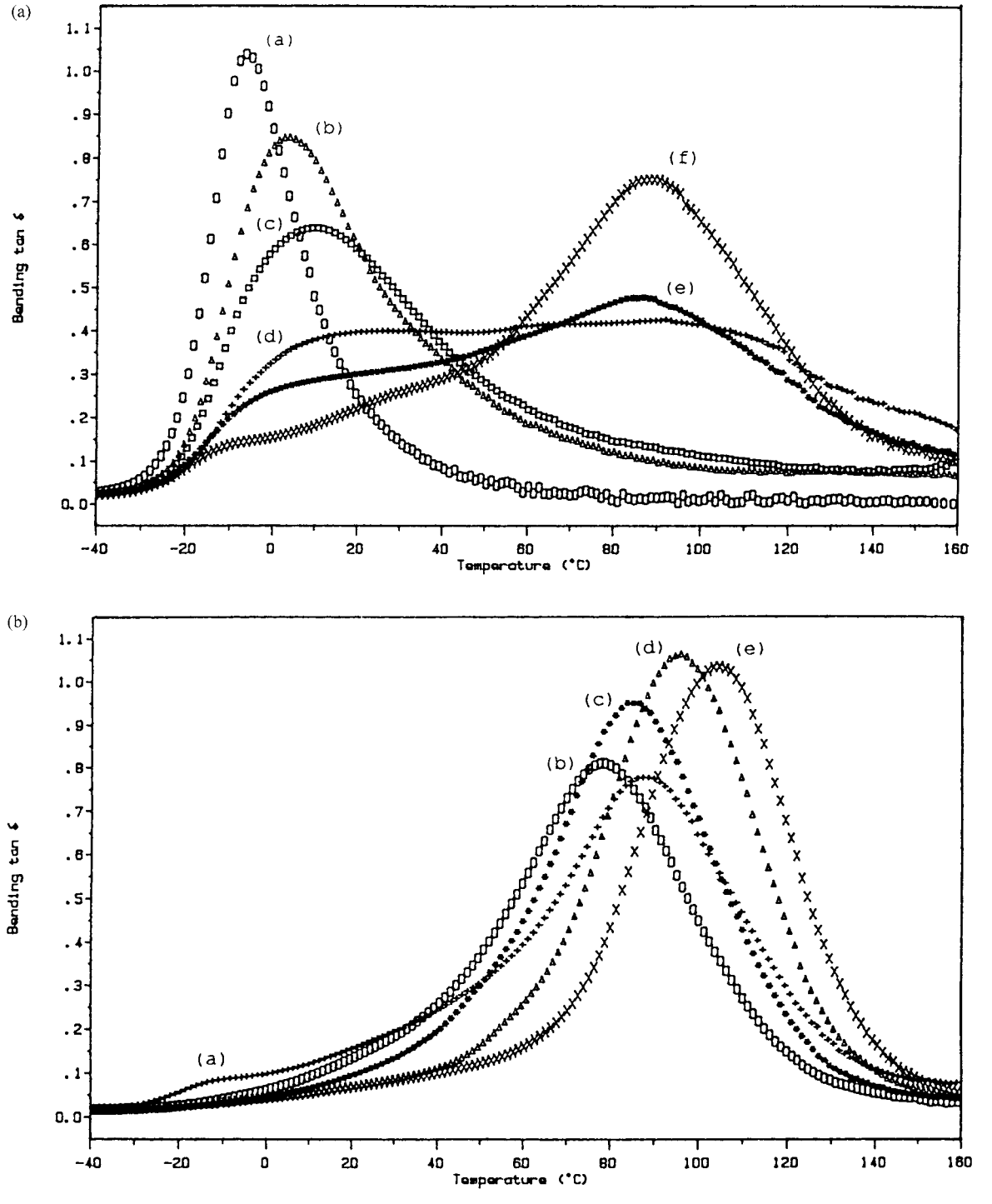

Fig. 6. Loss factor vs. temperature plots for the PUR/PEMA IPN compositions (*i*). (a) 100% PUR, (b) 90 : 10 PUR/PEMA, (c) 80 : 20, (d) 70 : 30, (e) 60 : 40, (f) 50 : 50; (ii): (a) 40 : 60, (b) 30 : 70, (c) 20 : 80, (d) 10 : 90 and (e) 100% PEMA.

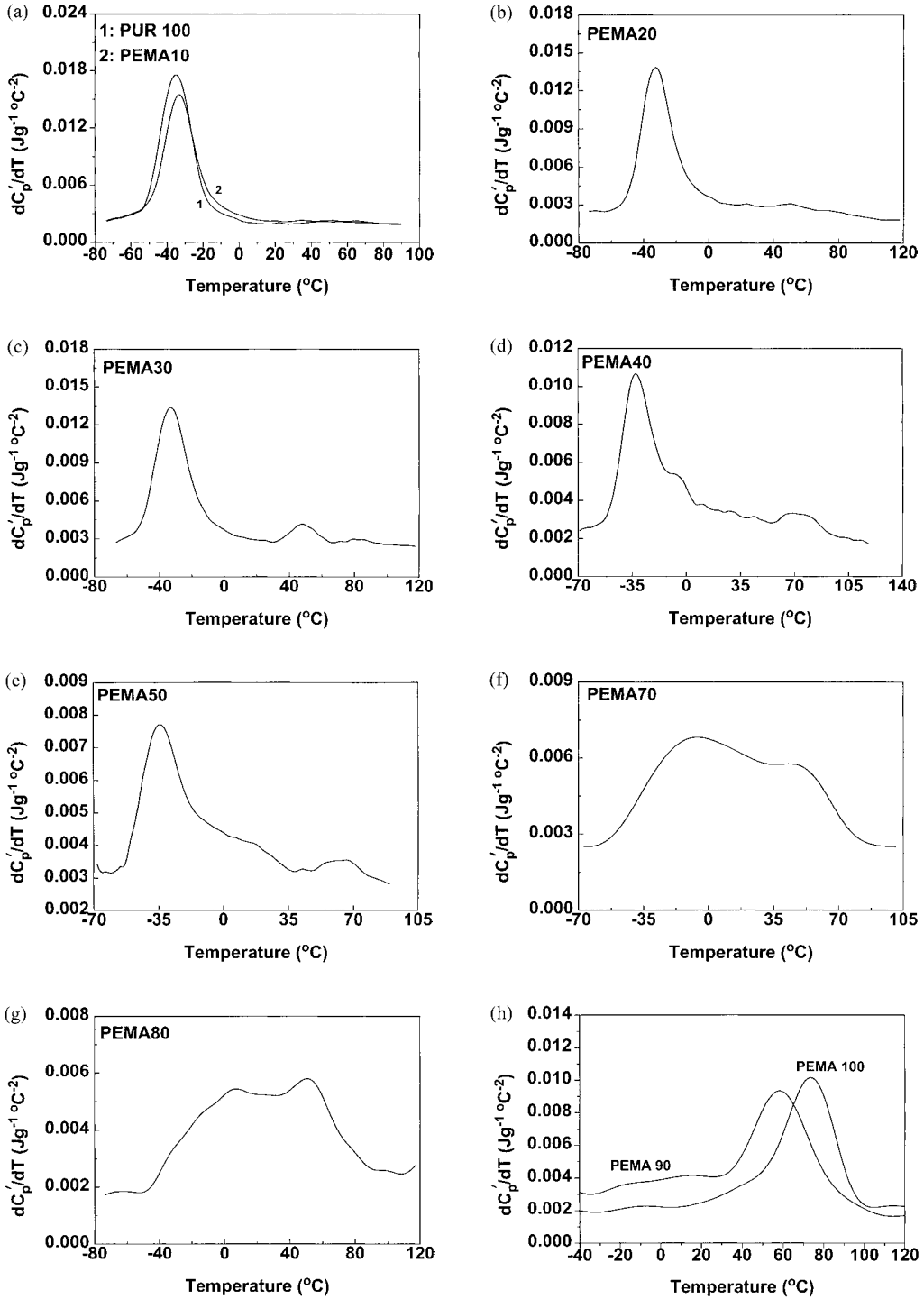

Fig. 7. dC_p'/dT vs. temperature plots for the PUR/PEMA IPNs. PEMA0, PEMA10, PEMA20, PEMA30, PEMA40, PEMA50, PEMA70, PEMA80, PEMA90 and PEMA100.

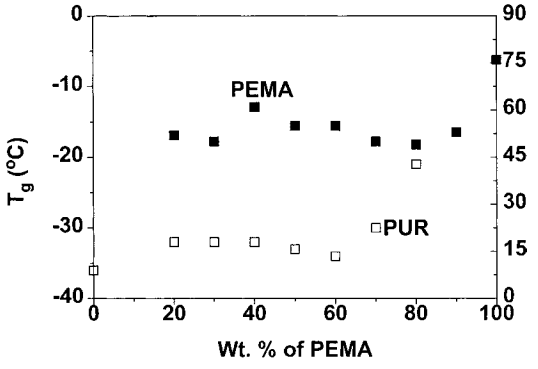

Fig. 8. T_g vs. composition for the PUR/PEMA IPNs. From M-TDSC data.

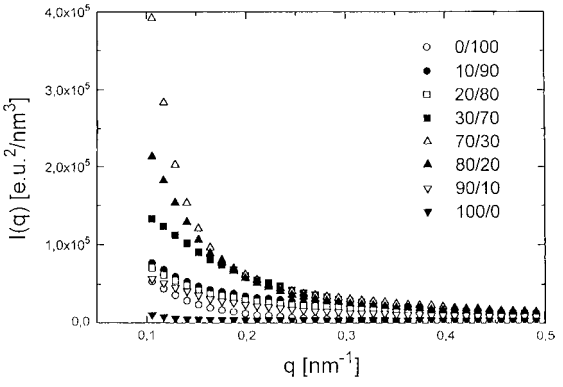

Fig. 9. Scattering intensity $I(q)$ vs. scattering vector, **q**, for the PUR/PEMA IPNs.

This implies that the phase separation occurring together with the IPN-forming reactions is not fully accomplished on account of restricted diffusion/viscosity.

3.2. Small-angle X-ray scattering

The relation between the absolute scattering intensities, $I(q)$, from SAXS measurements and the derived structure factor, $S(q)$, is given as follows.

$$I(q) = V_z \Delta h^2 S(q)$$

The scattering vector, **q**, is defined as

$$\mathbf{q} - 4\pi/\lambda \sin\theta$$

Here, V_z denotes the volume per repeat unit of the IPN, and Δh the electron density difference between the IPN phases, which can be determined from the experimental data by numerical integration [23].

The $I(q)$ vs. scattering vector **q** data are shown in Fig. 9. For the 100 : 0, 90 : 10, 80 : 20, 70 : 30, 30 : 70, 20 : 80 and 10 : 90 PUR/PEMA IPNs there is an increase at small q values, which indicates the existence of heterogeneous morphologies. For the PEMA 30 and PEMA20 samples, the increase in scattering intensity with decreasing q is much larger than for other samples.

The log–log plots of $I(q)$ vs. **q** are shown in Fig. 10. The scattering intensities for all samples cannot be described by a $q^{-\chi}$ dependence, which corresponds to the well-known Porod law [24] for the entire range of q; moreover, χ is a positive constant. At small q values, χ is smaller than at large q values.

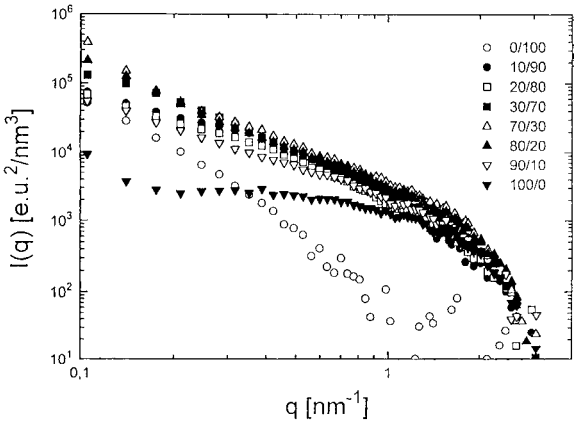

Fig. 10. $\log I(q)$ vs. $\log q$ for the PUR/PEMA IPNs.

The scattering profiles of the IPNs in Fig. 11(a) and (b) show the expected maximum in scattering intensity. All samples seem to have a complex morphology. From Fig. 11, it can be seen that the distribution of microdomain sizes is quite broad. The average size of domains is from 5–12 nm. These values may correspond to the average length of the frozen composition fluctuation that occur during IPN formation. For the PEMA10, PEMA70, PEMA80 and PEMA90, having one T_g indicated by DMTA experiments, no microphase separation can be resolved. This indicates that the resolution of DMTA is not sufficient for the analysis of the morphologies of the IPN series.

Alig et al. [23] studied simultaneous IPNs by means of SAXS. They proposed a new structure factor, $S(q)$, which reflects the development of a microphase struc-

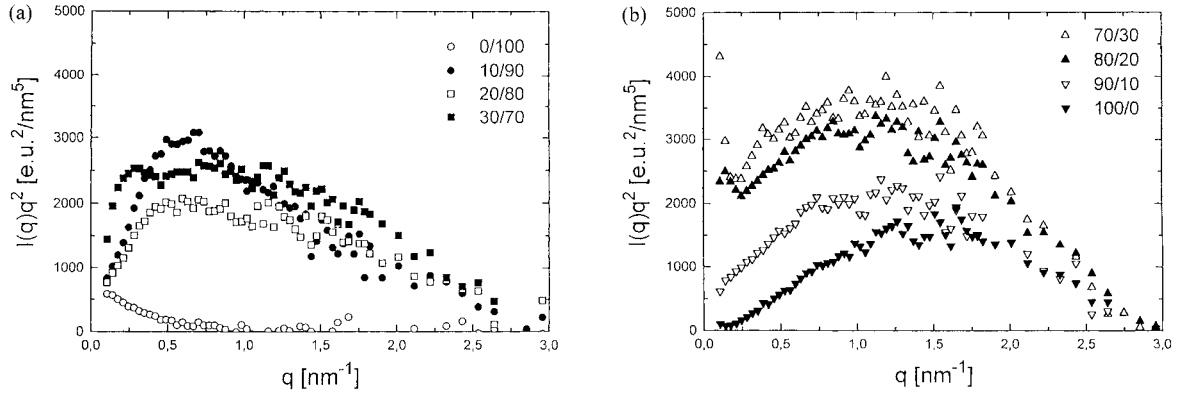

Fig. 11. Scattering intensity $I(q)q^2$ vs. q for the PUR/PEMA IPNs.

ture during the formation of simultaneously cross-linked IPNs:

$$S(q) = (1 - \exp(-\gamma q^2/S_0))S_0/q^2$$

with

$$S_0 = 1/[Aq^2 + m + C/q^2]$$

Here, A, m and C are time-average effective values [23], γ a new effective coefficient which depends on the diffusion coefficient of the monomers, the composition ratio and the kinetics of the IPN formation determined by τ_c. For the kinetics of the chemical reactions taking place during the IPN formation, there exists a finite time, $t = \tau_c$, above which the separation kinetics of the IPN is suppressed [23]. They used the new structure factor to achieve good fits with experimental data because the simultaneously cross-linked IPNs have a very fine morphology. The shapes of the scattering profile ($I(q)q^2$ vs, q), shown in Alig's paper [23], give a characteristic maximum scattering peak. However, the shapes of the scattering profiles of these IPNs (see Fig. 11(a and b)) are quite broad. It is difficult for us to use the new structure factor to analyse these experimental data. The broad scattering peak may be related to composition distribution. It is necessary to develop a new model for the data analysis.

3.3. Model experiment for analysis of morphology of IPNs

The real part of the heat capacity for polymers can be expressed as follows:

$$C'_p = A + BT + F(T) \tag{21}$$

Here, A and B are constants and $F(t)$ a function of temperature. Outside the transition region, $F(T) = 0$. For dC'_p/dT, the following relation holds:

$$dC'_p/dT = B + dF(T)/dT \equiv B + \phi(T) \tag{22}$$

As shown earlier, for polymers and miscible polymer blends, the dC'_p/dT vs. temperature signal can be described by a Gaussian function, G, of temperature, the increment of heat capacity, ΔC_p, the glass-transition temperature, T_g, and the half width of the glass-transition peak (from dC'_p/dT), ω_d.

$$G = \Delta C_p/[\omega_d(\pi/2)^{1/2}]\exp[-2(T - T_g)^2/\omega_d^2] \tag{23}$$

For a heterogeneous IPN, it is possible to consider G as a multiple Gaussian function in the transition region:

$$\begin{aligned} G &= \Sigma G_i(T, T_{gi}, \omega_{di}, \Delta C_{pi}) \\ &= \Delta C_{p1}/[\omega_{d1}(\pi/2)^{1/2}]\exp[-2(T - T_{g1})^2/\omega_{d1}^2] \\ &\quad + \Delta C_{p2}/[\omega_{d2}(\pi/2)^{1/2}]\exp[-2(T - T_{g2})^2/\omega_{d2}^2] \\ &\quad + \Delta C_{p3}/[\omega_{d3}(\pi/2)^{1/2}]\exp[-2(T - T_{g1})^2/\omega_{d3}^2] \\ &\quad + \dots \end{aligned} \tag{24}$$

$G_i(T)$ is related to the ith phase of the multi-phase system. For a multi-phase IPN, the total ΔC_p is the sum of ΔC_{pi} of each phase:

$$\Delta C_p = \Sigma \Delta C_{pi} \tag{25}$$

By a peak resolution technique, the parameters, ω_{di}, ΔC_{pi} and T_{gi} can be obtained.

For a phase separated system of two polymers, consider the polymer-1-rich phase. Its glass transition temperature, $T_g(1)$, and its increment of heat capacity, $\Delta C_p(10)$, are given theoretically as follows:

$$T_g(1) = w(1)^{(10)} T_g(1) + w(2)^{(10)} T_g(2) \quad (26)$$

$$\Delta C_p(10) = w(1)^{(10)} \Delta C_p(1) + w(2)^{(10)} \Delta C_p(2) \quad (27)$$

Thus, the weight fraction of polymer-1-rich phase, $w(1)$, is:

$$w(1) = \Delta C_p^{(1)} / \Delta C_p^{(10)} \quad (28)$$

Here, $w(1)^{(10)}$ and $w2^{(10)}$ are the weight fractions of polymers 1 and 2 in the polymer-1-rich phase, and $\Delta C_p{}^{(1)}$ the increment of heat capacity measured by peak resolution for the polymer-1-rich phase. According to Eq. (28), the weight fractions of other phases can be obtained as follows.

$$w(i) = \Delta C_p^{(i)} / \Delta C_p^{(i0)} \quad (29)$$

To evaluate the model, a four-component system was devised. This system comprised poly(methyl acrylate)/poly(vinyl acetate) (PMA/PVAc) physical blends, i.e. PMA/PVAc (80/20)+PMA/PVAc (60/40)+PMA/PVAc (40/60)+PMA/PVAc (20/80, wt/wt). Fig. 12 shows the change of experimental dC_p'/dT with temperature. The difference between glass transition temperature of PMA and PVAc is ca. 35°C. The transition signal of the four-component system in the glass-transition region showed an overlapping set of transition peaks. The solid and dashed lines are the

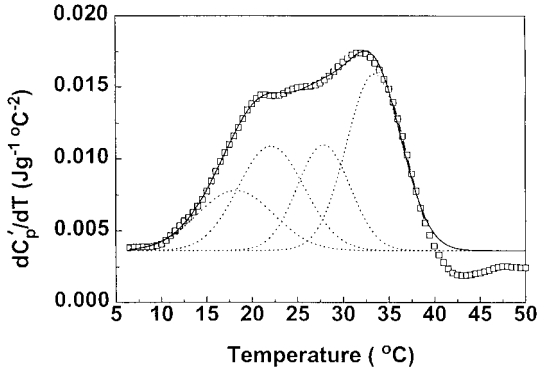

Fig. 12. Experimental data with peak resolution results for the four-component system.

Table 2
Comparison of experimental with calculated compositions

System	Experimental (wt%)	Calculated (wt%)
PMA-20	30	27.8
PMA-40	23	21.1
PMA-60	25	22.9
PMA-80	22	19.7

peak resolution results. Table 2 gives the comparison of the results by known weight and by calculation. The average deviation is ca. 8%.

3.4. Analysis of phase structure of IPNs

Based on DMTA measurements [22], one can judge the level of compatibility of multi-component polymeric materials. However, it is impossible by this technique to determine the concentration distribution and weight fraction in partially compatible systems.

Consider that a partially compatible IPN morphology can be divided into several phases: polymer-1-rich(1), polymer-2-rich(1), polymer-1-rich(2), polymer-2-rich(2) and interfacial phases. Comparing the behaviour of the dC_p'/dT vs. temperature from IPNs and that from the standard interface [25], it is hard to separate the interfacial phases from multiple phases for the PEMA10 to PEMA90 IPNs. So, we have to consider the interface in these IPNs as a phase, which has an average concentration.

Fig. 13(a–c) show the peak-resolution results for the PEMA30, PEMA40, PEMA50, PEMA60 and PEMA70 IPNs.

Also, comparisons of the dC_p/dT vs. temperature signal for the PEMA60 IPN and for a PEMA(60%)+PUR(40%) physical blend, for the PEMA70 IPN and for a PEMA(70%)+PUR(30%) physical blend are shown in Figs. 14 and 15.

In case of the PEMA70 and PEMA30 IPNs, three transition peaks were separated which may show three types of phase structure. For the PEMA40, PEMA50 and PEMA60 IPNs, four transition peaks were obtained. It is possible that, starting from the one-phase mixture of monomers, cross-linkers, initiators and catalysts, the chemical polymerisation and cross-linking reactions lead to growing network fragments and, meanwhile, the two network component start to phase separate due to thermodynamic immiscibility.

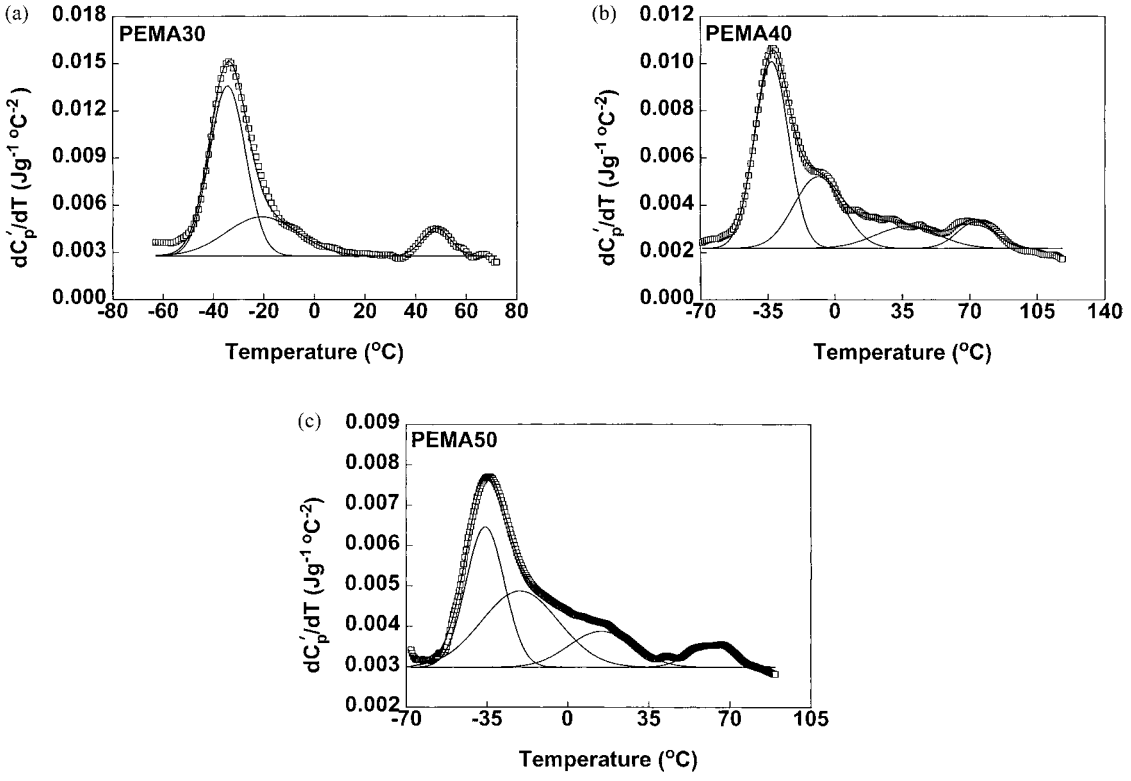

Fig. 13. Experimental data with peak resolution results for the PEMA30, PEMA40 and PEMA50 IPNs.

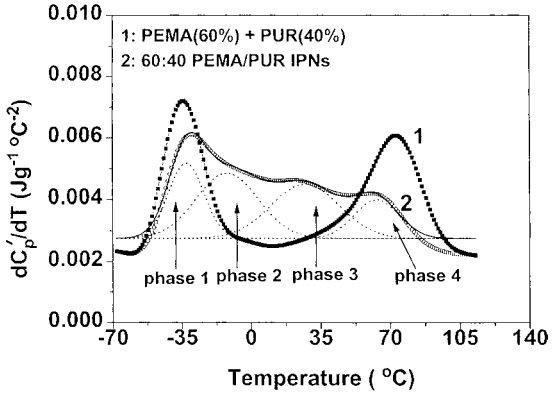

Fig. 14. dC_p'/dT vs. temperature for the PEMA60 IPN and for a PEMA(60%)+PUR(40%) physical blend.

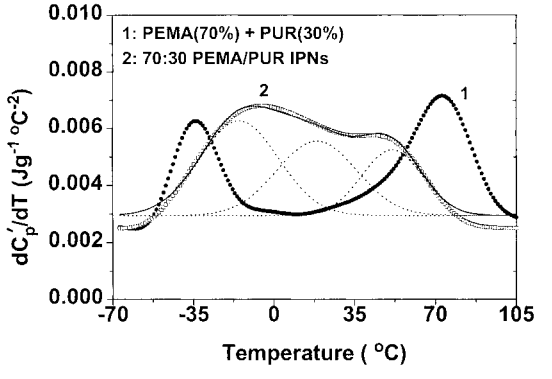

Fig. 15. dC_p'/dT vs. temperature for the PEMA70 IPN and for a PEMA(70%)+PUR(30%) physical blend.

From the M-TDSC and SAXS results, it is possible to believe that the polymerisation process does not lead only to two kinds of network fragments and an interfacial phase. It may lead to a very complex morphology with large local concentration fluctuations.

The degree of mixing in the IPNs can be analysed based on the dC_p'/dT vs. temperature signal. Table 3 gives an example of the PEMA60 IPN for which a four-component morphology was obtained. For the PUR-rich phases in the IPN, the weight fraction of

Table 3
Composition distribution for the PEMA60 IPN

System	T_g(°C)	Weight fraction (wt%)
Phase 1	−33	19.2
Phase 2	−12	29.8
Phase 3	27	30.4
Phase 4	63	16.1

19.2% is related to a glass-transition temperature of −33°C and 29.8% to a glass-transition temperature of −12°C. For the PEMA-rich phases, the weight fraction of 30.4% related to a glass-transition temperature of 27°C and 16.1% to a glass-transition temperature of 63°C. Combining M-TDSC and DMTA experiments, it is possible to analyse the relationship between morphology, structure and mechanical properties of IPNs better than before.

4. Conclusions

M-TDSC data showed that the morphology of the PEMA/PUR IPNs was multi-phase in nature. SAXS results indicated that the domain size distribution of the PEMA/PUR IPNs was quite broad. By using the dC'_p/dT signal from M-TDSC experiments and a peak resolution technique, the phase structure of IPNs can be analysed, and phase wight fractions can be obtained. This provides a new method for a more detailed analysis of IPNs than has been possible to date.

Acknowledgements

The authors gratefully thank Professor I. Alig at Deutsches Kunststoff Institute, Germany, for considerable help with the SAXS measurements and data analysis.

References

[1] L.H. Sperling, Interpenetrating Polymer Networks and Related Materials, Plenum Press, New York, 1981.
[2] J.H. An, L.H. Sperling, in R.A. Dickie, S.S. Labana, R.S. Bauer (Eds.), Cross-linked Polymers, ACS Series 376, American Chemical Society, Washington, DC, 1988.
[3] D. Klempner, J. Berkowski, in H. Mark, N.M. Bikales, C.G. Overberger, G. Menges (Eds.), Encyclopedia of Polymer Science and Engineering, Vol. 8, John Wiley & Sons, New York, 1988.
[4] H.L. Frisch, D. Klempner, H.K. Yoon, K.C. Frisch, Macromolecules 13 (1980) 1016.
[5] M.M. Coleman, C.J. Serman, P.C. Painter, Macromolecules 20 (1987) 226.
[6] B.J. Bauer, M.R. Briber, C.C. Han, Macromolecules 22 (1989) 940.
[7] B.J. Bauer, M.R. Briber, in D. Klempner, K.C. Frisch (Eds.), Advances in Interpenetrating Polymer Networks, Vol. 4, Technomic, Lancaster, PA, USA, 1994.
[8] M. Akay, S.N. Rollins, Polymer 34 (1993) 1865.
[9] B.McGarey, in D. Klempner, K.C. Frisch (Eds.), Advances in Interpenetrating Polymer Networks, Vol. 1, Technomic, Lancaster, PA, USA, 1989.
[10] Y. Lipatov, in D. Klempener, K.C. Frisch (Eds.), Advances in Interpenetrating Polymer Networks, Vol. 1. Technomic Publishing Co. Lancaster, PA, USA, 1989.
[11] A. Alig, M. Junker, W. Jeninger, H.L. Frisch, M. Schulz, Morphology of Polymers Conference, Prague, 1995.
[12] A.J. Kovacs, J.M. Hutchison, J. Polym. Sci. Polym. Phys. 14 (1976) 1575.
[13] M. Reading, Trends in Polymer Science 1 (1993) 249.
[14] A.A. Lacey, C. Nikolopoulos, H.M. Pollock, M. Reading, to appear in J. Thermal Anal.
[15] M. Reading, R. Wilson, H.M. Pollock, J.B. Enns (Ed.), Proceeding of the 23rd NATAS Conference, Toronto, 1994, pp. 2–7.
[16] M. Song, A. Hammiche, H.M. Pollock, D.J. Hourston, M. Reading, Polymer 36 (1995) 3133.
[17] A. Savitsky, M.J.E. Golay, Anal. Chem. 36 (1964) 1627.
[18] V. Huelck, D.A. Thomas, L.H. Sperling, Macromolecules 5 (1972) 340.
[19] D.J. Hourston, F.U. Schafer, J. Polym. Adv. Technol., Special Edition IPNs 7 (1996) 273.
[20] M.T. Tabka, J.M. Widmaier, G.C. Meyer, Plastic, Rubber Composition Processing Applications 16 (1991) 11.
[21] V. Mishra, F.D. Frez, L.H. Sperling, J. Polym. Mat. Sci. Eng. 16 (1995) 124.
[22] F.U. Schafer, Ph.D. Thesis, Loughborough University, UK, 1996.
[23] I. Alig, M. Junker, M. Schulz, H.L. Frisch, in press.
[24] G. Porod, Kolloid Z. 124 (1951) 83; 125 (1952) 51; and 125 (1952) 108.
[25] M. Song, D.J. Hourston, A. Hammiche, H.M. Pollock, M. Reading, Polymer 38 (1997) 1.